LETTER

doi:10.1038/nature10985

# Genome-wide protein–DNA binding dynamics suggest a molecular clutch for transcription factor function

Colin R. Lickwar[1]*, Florian Mueller[2,3]†*, Sean E. Hanlon[1]†, James G. McNally[2] & Jason D. Lieb[1]

**Dynamic access to genetic information is central to organismal development and environmental response. Consequently, genomic processes must be regulated by mechanisms that alter genome function relatively rapidly[1–4]. Conventional chromatin immunoprecipitation (ChIP) experiments measure transcription factor occupancy[5], but give no indication of kinetics and are poor predictors of transcription factor function at a given locus. To measure transcription-factor-binding dynamics across the genome, we performed competition ChIP (refs 6, 7) with a sequence-specific *Saccharomyces cerevisiae* transcription factor, Rap1 (ref. 8). Rap1-binding dynamics and Rap1 occupancy were only weakly correlated ($R^2 = 0.14$), but binding dynamics were more strongly linked to function than occupancy. Long Rap1 residence was coupled to transcriptional activation, whereas fast binding turnover, which we refer to as 'treadmilling', was linked to low transcriptional output. Thus, DNA-binding events that seem identical by conventional ChIP may have different underlying modes of interaction that lead to opposing functional outcomes. We propose that transcription factor binding turnover is a major point of regulation in determining the functional consequences of transcription factor binding, and is mediated mainly by control of competition between transcription factors and nucleosomes. Our model predicts a clutch-like mechanism that rapidly engages a treadmilling transcription factor into a stable binding state, or vice versa, to modulate transcription factor function.**

The diverse biological functions of Rap1 (ref. 9) make it an excellent model for testing the hypothesis that binding dynamics are important for transcription factor function (Supplementary Fig. 1). We developed a strain with two copies of *RAP1*. One copy of *RAP1* was tagged with a 3× Flag epitope and was constitutively expressed from the endogenous *RAP1* promoter. A second copy of *RAP1* was tagged with a 9× Myc epitope and was controlled by a weakened galactose-inducible promoter, *GALL* (an attenuated version of the *GAL1* promoter) (Fig. 1a). This strain showed no growth defects in inducing (2% galactose) or non-inducing (2% dextrose) conditions (Fig. 1b and Supplementary Fig. 2). To avoid cell-cycle and DNA replication effects, for the duration of the experiment the strain was arrested in G1 with alpha factor[6]. The induced Rap1 protein isoform could be detected as early as 30 min after galactose induction (Fig. 1c). The ratio of Rap1 isoforms provided an estimate of the nucleoplasmic pool of Rap1 molecules (Fig. 1d). We then performed Myc and Flag ChIP experiments independently from extract corresponding to each of 10 time points (0, 10, 20, 30, 40, 50, 60, 90, 120 and 150 min after induction). We also performed ChIP to measure total Rap1 occupancy using a Rap1-specific antibody at 0 and 60 min. DNA fragments enriched in the ChIPs were detected on whole-genome-tiling 12-plex microarrays containing 270,000 probes per subarray, with an average probe interval of 41 bp and an average probe length of 54 bp (Supplementary Fig. 3). The entire time-course experiment was performed in duplicate. (Procedural details can be found in the Methods.)

After induction, Rap1–Myc was incorporated at targets where Rap1 had previously been shown to bind[8,10] (Fig. 2a, b), indicating that the system was functioning as designed. The increase in Rap1 protein caused by the induction of the competitor did not cause an increase in the overall occupancy at the measured Rap1 sites (Fig. 2c, d and Supplementary Figs 4 and 5). As Rap1–Myc ChIP occupancy increased at sites of Rap1 binding, Rap1–Flag occupancy decreased coordinately (Fig. 2c, d and Supplementary Fig. 4). Thus, Rap1–Myc is competing specifically with Rap1–Flag at each locus, and Rap1–Myc binding is not the result of cooperativity or additional Rap1 binding locations.

To interpret our data, we developed a model to determine turnover rates of Rap1 by modifying a fitting algorithm used previously to

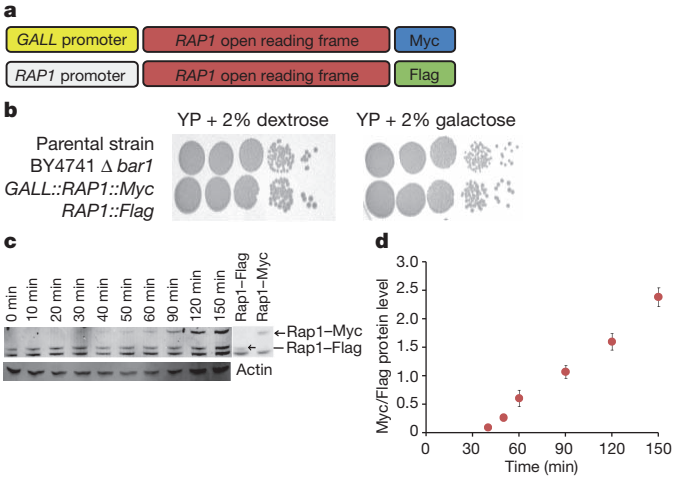


**Figure 1 | Development of transcription factor competition ChIP yeast strains.** **a**, Schematic of the Rap1 competition-ChIP yeast strain. **b**, Growth comparison of competition yeast strain and wild-type in inducing (2% galactose) and non-inducing (2% dextrose) conditions. **c**, Western blot analysis using an antibody against Rap1 (y-300). Strains containing only a Rap1–Myc or only Rap1–Flag copy are shown to the right to indicate the size of isoform-specific bands. The actin loading control is shown below. **d**, To estimate the dynamics of induction, the ratio of induced Rap1–Myc and constitutive Rap1–Flag protein is plotted. Data are from two technical replicates of two independent time-course replicates. Error bars represent s.e.m.

[1]Department of Biology, Carolina Center for the Genome Sciences, Curriculum in Genetics and Molecular Biology, and Lineberger Comprehensive Cancer Center, CB 3280, 408 Fordham Hall, University of North Carolina at Chapel Hill, Chapel Hill, North Carolina 27599-3280, USA. [2]LRBGE-National Cancer Institute, The National Institutes of Health, 41 Library Drive, Bethesda, Maryland 20892, USA. [3]Institut Pasteur, Groupe Imagerie et Modélisation, Centre National de la Recherche Scientifique, Unité de Recherche Associée 2582, 25-28 rue du Docteur Roux, 75015 Paris, France. †Present addresses: Institut de Biologie de l'Ecole Normale Supérieure, Functional Imaging of Transcription, Centre National de la Recherche Scientifique, Unité Mixte de Recherche 8197, 45 rue d'Ulm, 75005 Paris, France (F.M.); Office of Physical Sciences-Oncology, CSSI, NCI, NIH, 31 Center Drive, Room 10A03, Bethesda, Maryland 20892, USA (S.E.H.).
*These authors contributed equally to this work.

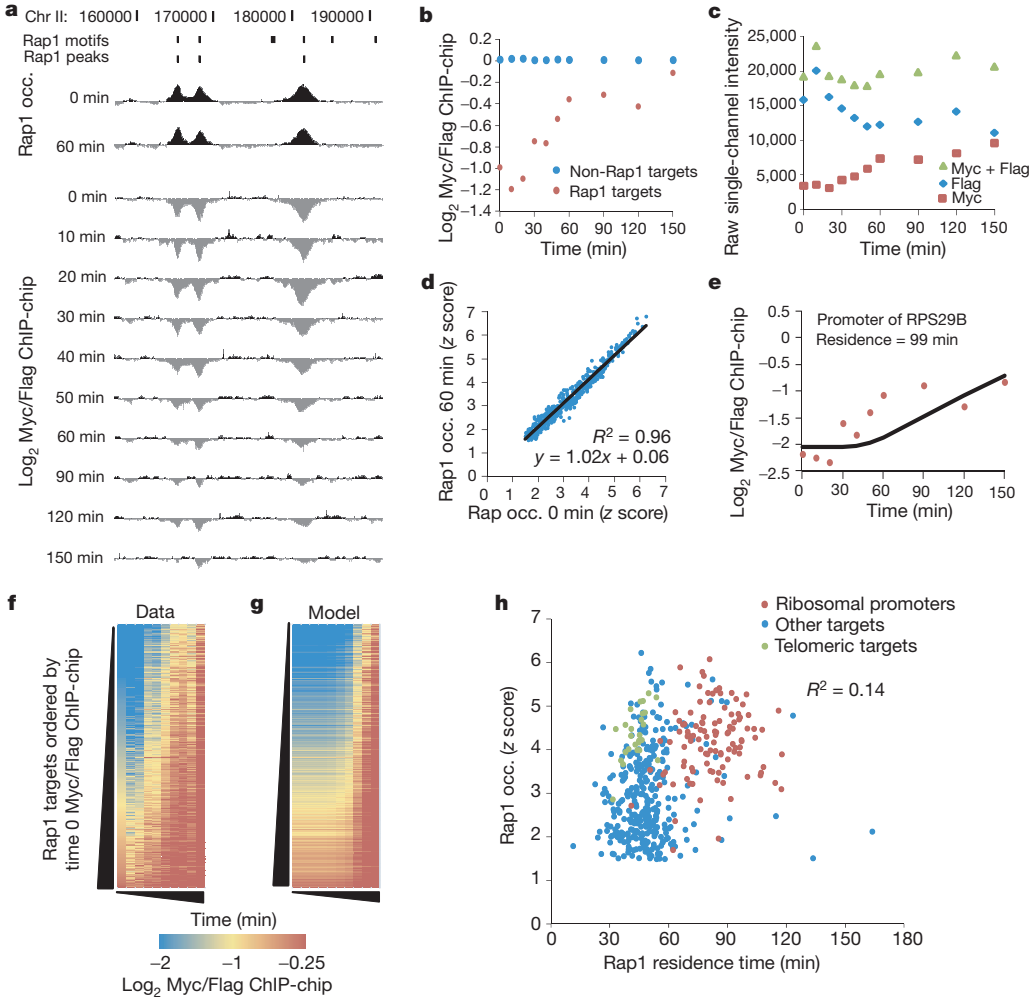


**Figure 2 | Rap1-bound sites exhibit distinct replacement dynamics.** **a**, A Rap1 turnover experiment over a 30-kb region of chromosome II (Chr II). Rap1 motifs and peaks are shown. **b**, Average $\log_2$ Myc/Flag ratio values for all Rap1 targets (red) increase relative to non-Rap1 targets (blue). **c**, Rap1–Myc competes with Rap1–Flag for binding. Average single-channel intensity for Rap1–Myc and Rap1–Flag for a single probe (CHR15FS000978891) in the promoter of the *TYE7* gene shows that the increase in Rap1–Myc is coincident with the loss of Rap1–Flag. **d**, Total Rap1 occupancy does not change during the time course. Average total Rap1 occupancy (occ.) ($\log_2$ ratio of Rap1 immunoprecipitation (y-300) to input ratio *z* score) at Rap1 targets at time 0 is plotted against that at 60 min. **e**, Average $\log_2$ Myc/Flag ratios for the promoter of ribosomal protein gene *RPL29B* (red points). The model fit for the residence time parameter that best fits these data is shown (black line). **f**, Colorimetric representation of $\log_2$ Myc/Flag ratios for all 465 Rap1 targets, sorted by the initial (normalized) $\log_2$ Myc/Flag ratio. **g**, For each site in **f**, the $\log_2$ Myc/Flag ratio predicted by our residence model, based on the calculated residence time, is shown. **h**, Rap1 occupancy (time 0 *z* score) versus Rap1 residence for 465 Rap1 targets ($R^2 = 0.14$, 0.37; Spearman rank correlation).

measure histone H3 turnover[6]. Under our experimental conditions, the extracted turnover rate for a transcription factor at a binding site is equivalent to its dissociation rate, which allows us to measure the residence time (Supplementary Figs 6–8 and Supplementary Text). Our experimental system can quantify binding events that have an apparent duration of 500 s or longer (Supplementary Figs 6 and 7, and Supplementary Text). Using our ChIP data and model we measured residence time of Rap1 at 439 peaks of Rap1 enrichment genome-wide, and at the 26 uniquely mappable telomeres (Fig. 2e–h, Supplementary Fig. 9 and Supplementary Text). Rap1 occupancy correlated only modestly with Rap1 residence ($R^2 = 0.14$; Spearman rank correlation = 0.37) (Fig. 2h), and distinct dynamics of Rap1–Myc incorporation were observed at different genomic loci (Fig. 2e–h). Thus, residence time and occupancy are distinct measurements, and our system was capable of distinguishing Rap1 turnover kinetics at different loci in the same experiment.

We found that efficient transcriptional activation was associated with stable Rap1 binding, whereas lower transcript production was associated with treadmilling, despite similar levels of Rap1 occupancy. Long Rap1 residence times occurred at ribosomal protein gene promoters, which are very highly transcribed and strongly activated by Rap1 (refs 6, 11, 12) (Fig. 2e, h). In contrast, Rap1 binding to non-ribosomal protein targets and to the infrequently transcribed telomeric and subtelomeric Rap1 sites was characterized by fast turnover (Fig. 2h and Supplementary Figs 10 and 11). Stable Rap1 binding seems to support higher mRNA production through more efficient recruitment of the RNA polymerase II machinery[12] (Fig. 3a). Genes with stable Rap1 binding at their promoters indeed exhibited high levels of RNA polymerase II association[6] (Fig. 3a), high transcription initiation rates[11,13] (Fig. 3b) and high mRNA levels (Fig. 3c). Rap1 occupancy does not correspond as strongly (Fig. 3a–c; right panels). TATA-binding protein (TBP) turnover[7] is also slow at ribosomal protein genes, indicating that slow transcription-factor-binding dynamics may be a hallmark of efficient transcription initiation[11,13].

We next examined possible mechanisms for the locus-specific differences in Rap1 residence time. Nucleosomes are a major regulator of genome accessibility[14], so we examined the relationship between histone modification and Rap1-binding dynamics[15,16]. Sites of long Rap1 residence were strongly correlated with sites of enrichment for the histone acetyltransferases Gcn5 and particularly Esa1 (ref. 17) (Fig. 3d, e).

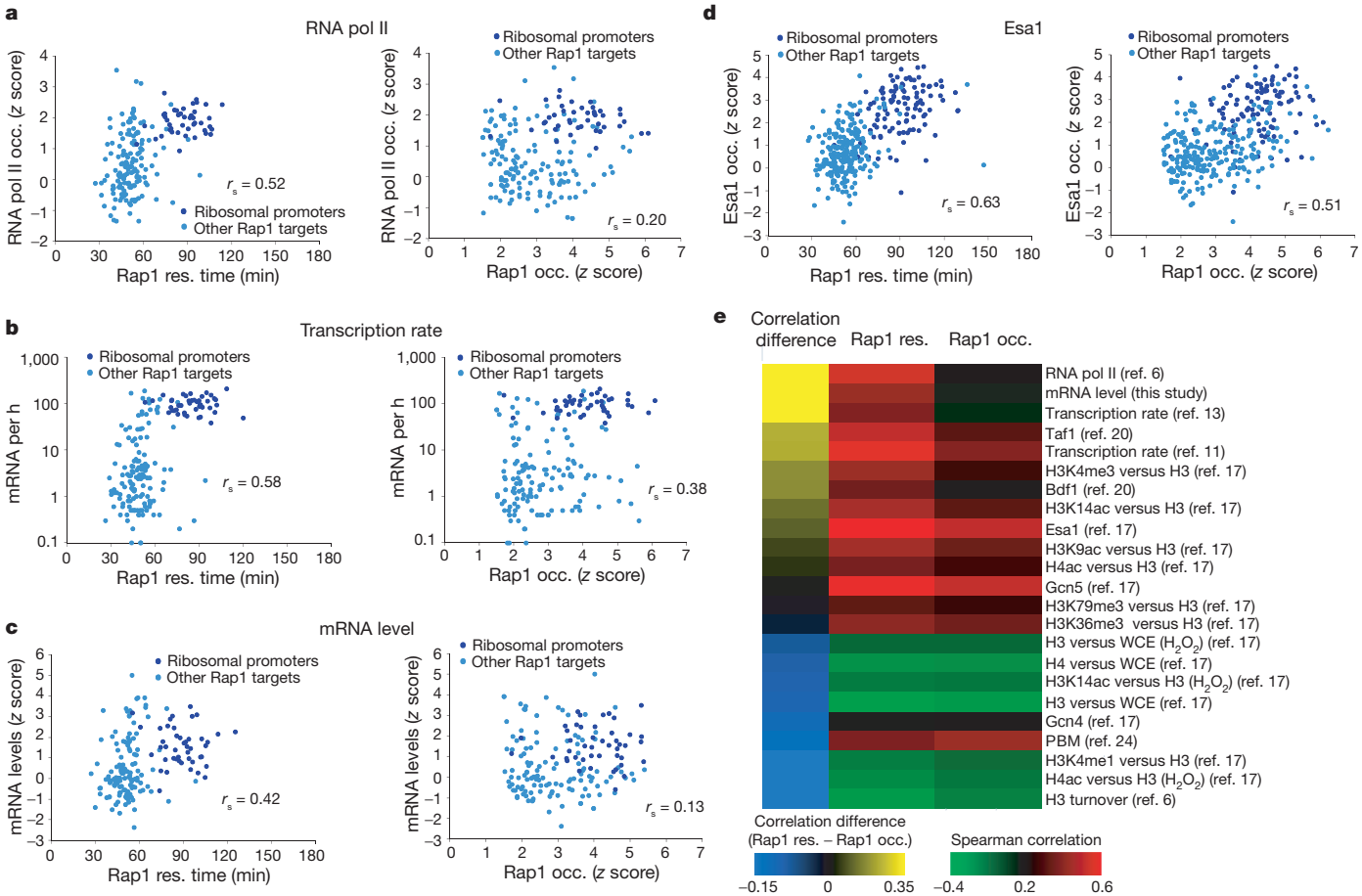


**Figure 3 | RNA polymerase II recruitment, mRNA production, and histone acetyltransferase recruitment is associated with long Rap1 residence.** **a**–**d**, Left, Rap1 residence (res.) time is plotted on the *x* axis. Right, Rap1 occupancy is plotted on the *x* axis. In both panels, the following are plotted on the *y* axis: RNA polymerase II (RNA Pol II) occupancy (**a**)[6]; the number of mRNA transcripts per h (**b**) (ref. 11); mRNA levels at time 0 (**c**); and histone acetyltransferase Esa1 occupancy *z* scores (**d**)[17]. $r_s$ is the Spearman correlation value. **e**, Colorimetric representation of the Spearman rank correlation between various genomic data sets and Rap1 occupancy (right) and Rap1 residence (centre), ordered by the magnitude of the difference between the residence and occupancy correlations for each comparison (left). WCE, whole-cell extract; PBM, protein-binding microarray. Telomeric targets are excluded from analysis (Supplementary Text).

Nucleosome instability reinforced by Gcn5 and Esa1 (members of SAGA and NuA4, respectively) may stabilize Rap1 binding by reducing competition with nucleosomes[18,19]. Other indicators of active promoters—including H3K4me3, occupancy by the bromodomain protein Bdf1 (similar to mammalian TAF1)[20], and acetylation of H3K9, H4 and H3K14—were also more strongly associated with Rap1 residence time than with Rap1 occupancy (Fig. 3e).

In general, sites that are bound by Rap1 are strongly depleted of nucleosomes[21]. However, the binding dynamics data allowed us to appreciate a more complex relationship. We grouped Rap1-bound loci into four categories based on their measured Rap1 residence time: longest, long, short, and shortest. We then aligned the Rap1 motifs in each category and plotted nucleosome occupancy relative to the motif position, reasoning that nucleosomes in direct proximity to the DNA motif bound by Rap1 would have a strong influence on Rap1 residence times[21]. As expected, strong nucleosome depletion was centred on the Rap1 motif (Fig. 4a). However, as Rap1-binding turnover increased, nucleosome depletion was correspondingly less pronounced. Thus, not all highly occupied Rap1 sites are equally depleted of nucleosomes *in vivo*. Instead, a subset of loci at which Rap1 occupancy is high but binding turnover is also high (treadmilling) are associated with higher nucleosome occupancy (Supplementary Fig. 11b). No consistent relationship is apparent when Rap1 targets are grouped by occupancy, as measured by traditional ChIP (Fig. 4a).

We next examined nucleosome occupancy on naked DNA in the absence of Rap1 or any protein cofactors[21]. Notably, DNA-encoded nucleosome occupancy measured *in vitro* is low only for the class of Rap1 targets with the most stable binding (Fig. 4b and Supplementary Fig. 11b). This pattern was not recapitulated when Rap1 targets were sorted by occupancy (Fig. 4b). This suggests that the nucleosome behaviour surrounding transcription factor motifs is at least partially encoded in DNA[15], and that this DNA-encoded nucleosome occupancy can influence the binding dynamics of transcription factors, and thereby affect functional outputs (Supplementary Fig. 11a–c).

We sought further evidence supporting direct competition between nucleosomes and Rap1. We compared histone H3 turnover[6] to Rap1 residence times and found that loci with long Rap1 residence times also had relatively slow H3 turnover. Similarly, histone H3 molecules that treadmill are found almost exclusively at sites of Rap1 treadmilling (Fig. 4c). Rap1–nucleosome interactions isolated by immunoprecipitating Rap1 after MNase digestion[22] were also detected more often at treadmilling sites (Fig. 4d). Further evidence for competition is supported by a marked increase in nucleosome occupancy directly over Rap1 motifs after Rap1 depletion[23] at treadmilling loci, but not at loci with stable Rap1 binding (Fig. 4e). These relationships provide evidence for direct competition between Rap1 and nucleosomes.

Given that high DNA-encoded nucleosome occupancy is associated with rapid Rap1 turnover (Fig. 4b), it is reasonable to expect that differences in the strength of the DNA motif bound by the transcription factor would also influence turnover. To test this, we examined the relationship between Rap1 turnover and experimentally measured *in vitro* Rap1 affinity at each locus[24]. For sites with longer Rap1 residence,

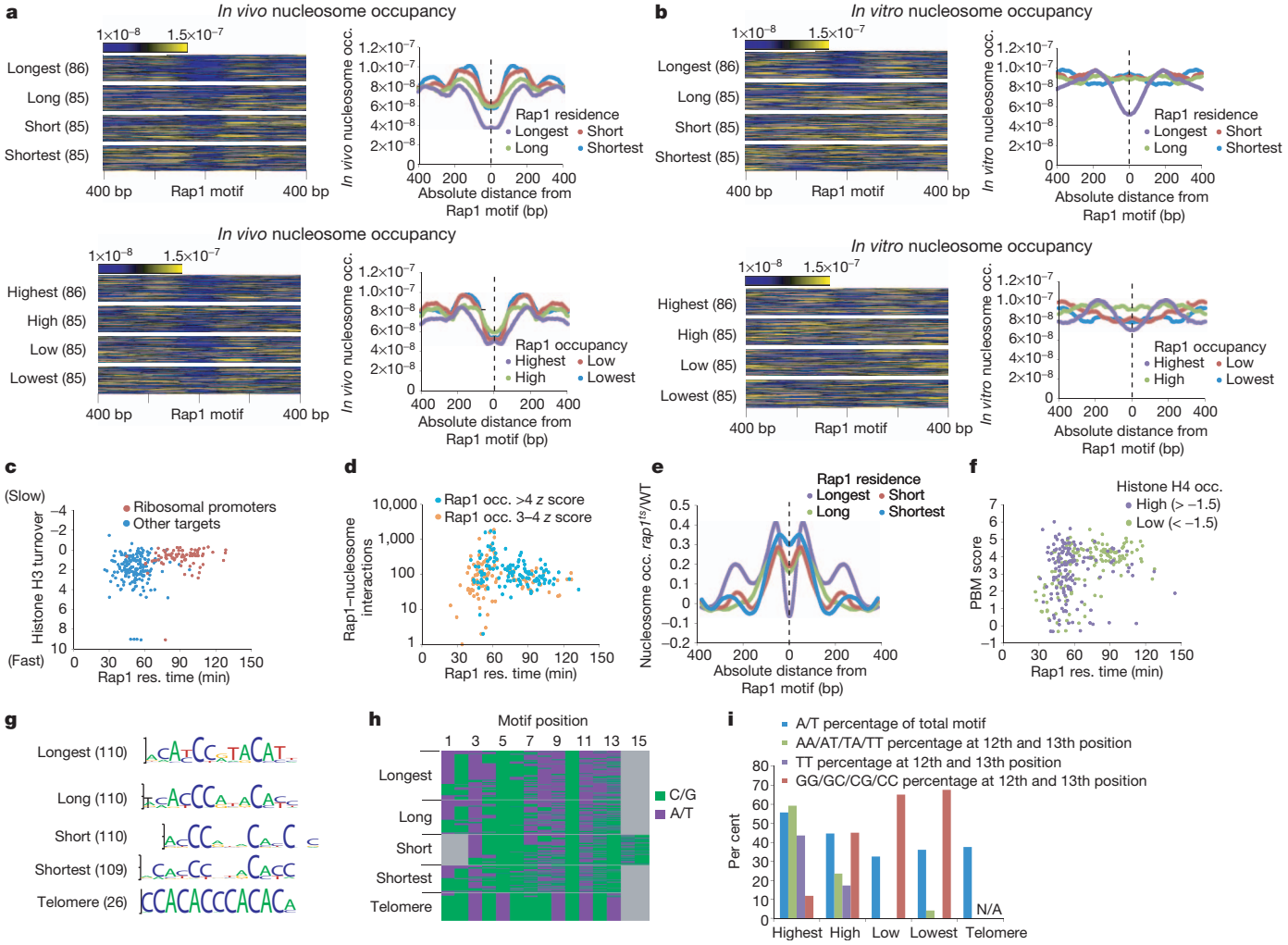


**Figure 4 | Evidence for competition between Rap1 and nucleosomes.** **a**, Colorimetric representation of *in vivo* nucleosome occupancy centred on Rap1-binding motifs. Loci are ordered by Rap1 residence time (top) or Rap1 occupancy (bottom). The total number of Rap1 targets in each group is shown in parentheses. To the right are plots of the average nucleosome occupancy for each group centred on the Rap1 motif. Targets with several Rap1 motifs are represented by one randomly chosen motif. **b**, Same as (**a**) but for *in vitro* nucleosome occupancy. **c**, Histone H3 turnover versus Rap1 residence for ribosomal protein genes (red) and other targets (blue). **d**, The number of Rap1–nucleosome interactions[22] detected within each Rap1 target peak boundary on a $\log_{10}$ scale. **e**, Relative change in nucleosome occupancy following Rap1 depletion[23] centred on Rap1 motifs grouped by residence time. A value of zero represents no relative change in nucleosome occupancy. **f**, *In vitro* Rap1 affinity for its cognate target, as measured using a PBM[24], compared to Rap1 residence. Colours represent histone H4 occupancy *z* scores ($>-1.5$ purple (high), $<-1.5$ green (low)[17]). **g**, Top-position weight matrix motifs discovered for Rap1 targets, grouped by residence. The number of targets for each group is in parentheses. **h**, All motifs from the top-position weight matrix for each residence group are coloured by their A or T (A/T) (purple), or G or C (G/C) (green) content at each motif base position. **i**, Percentage of A/T content for the entire motif (blue), AA/AT/TA/TT at the twelfth and thirteenth motif position (green), TT at the twelfth and thirteenth position (purple) and GG/GC/CG/CC at the twelfth and thirteenth position (red) for Rap1 targets, grouped by residence and telomeric regions.

Rap1's affinity for DNA was generally high, whereas Rap1 sites with the fastest turnover had lower experimentally measured Rap1 affinity (Fig. 4f). Despite this relationship, among sites with strong Rap1 motifs, nucleosome occupancy was still the major factor distinguishing sites with long Rap1 residence times from those with higher turnover (Fig. 4f).

Longer *in vivo* Rap1 residence times at sites of high Rap1 affinity are consistent with control of the Rap1–nucleosome competition being encoded directly in the DNA sequence to a substantial degree[15,16]. We reasoned that this would be reflected in the sequence of the DNA motifs bound by Rap1. Indeed, we found differences in the composition of the Rap1 motifs for each of the turnover categories, with the longest residence Rap1 sites preferentially containing A or T at positions 4, 8, 12 and 13 (Fig. 4g–i). These associations were not as strong when Rap1 targets were ordered by occupancy (Supplementary Fig. 12). Sites at which residence was shortest tended to contain a degenerate Rap1 binding motif (Fig. 4g).

For several other transcription factors, microscopy-based measurements at individual loci point to much shorter residence times than those measured for Rap1 (refs 1, 3, 4, 25–27). For example, despite an *in vitro* residence time similar to Rap1 (~90 min[9,28]), glucocorticoid-receptor binding seems to be exceptionally short-lived at individual loci[26,27]. Nevertheless, an overall positive relationship between residence time and transcriptional output is observed for both Rap1 and glucocorticoid receptor[3,29]. The differences in Rap1 and glucocorticoid-binding dynamics, and the disparity between glucocorticoid-receptor residence time *in vitro* and *in vivo*, may reflect different modes of interactions with nucleosomes. The binding affinity of glucocorticoid receptor may be particularly sensitive to nucleosome packaging or may be regulated by the availability of DNA that is transiently accessible from the nucleosome surface[18]. This type of accessibility on the nucleosome itself could be regulated, and would not rely on the complete loss of a nucleosome[14]. Rap1 itself exhibits such properties, with its binding progressively inhibited as the motif recognized by

Rap1 is moved closer to the nucleosome dyad[30]. Our data do not exclude a model in which transcription factor binding occurs adjacent to a nucleosome, and competition occurs without complete nucleosome eviction[14,22,30].

In this study, we determined Rap1-binding dynamics genome-wide using competition ChIP. Rap1 occupancy was only weakly correlated with Rap1 binding turnover, showing that these are independently measurable properties. Binding turnover correlates more strongly than occupancy with many aspects of genomic function, most predominantly RNA polymerase II recruitment and transcript levels. Stable Rap1 binding is associated with activation, whereas Rap1 treadmilling is associated with higher nucleosome occupancy, nucleosomal treadmilling, and a lack of transcription. Our work provides the basis for a model in which transcription-factor-binding dynamics is a major point of regulation in determining the functional consequences of transcription factor binding. Importantly, this model provides a plausible mechanism for a locus-specific switch between inactive and active transcription factor states, or even for a rapid switch from an activator (stable binding) to a repressor (treadmilling), or vice versa. This could be achieved at any given locus through a 'clutch' that alters the balance of the continual competition between transcription factors and nucleosomes (Supplementary Fig. 1). This clutch could operate through histone modification, histone-variant incorporation, ATP-dependent chromatin remodelling, cofactor binding, or any other site-directed chromatin altering activity.

## METHODS SUMMARY

**Strain construction.** The *RAP1* gene and promoter was cloned into the pRS403 plasmid and integrated by homologous recombination into the *HIS3* locus of the BY4741 *S. cerevisiae* strain. The two copies of *RAP1* were then sequentially tagged using the 9× Myc epitope from pYM20:hphNT1 at the *HIS3* copy of *RAP1* and the 3× Flag tag from p3Flag-KanMX at the endogenous *RAP1* copy. The *HIS3* copy of the *RAP1* promoter was replaced using homologous recombination by amplifying the GALL:*natNT2* promoter from the pYM-N27 plasmid. Integrations were confirmed using PCR and western blot analysis. The *BAR1* gene was knocked out by homologous recombination using a *LEU2* gene amplified from pRS405.

**Time course.** Yeast were grown overnight in YPD (yeast extract 1%, peptone 2% and dextrose 2%) and used to inoculate 800 ml of YPR (yeast extract 1%, peptone 2% and raffinose 2%) to an attenuance at 600 nm ($D_{600\ nm}$) of 0.2 (Genesys 20 Spectrophotometer) in a 4-l Erlenmeyer flask. These cells were grown to an $D_{600}$ of 0.4 and subsequently arrested using 5 μM alpha factor (400 μl of 10 mM, GenScript) until 95% of the yeast cells were unbudded (~3 h). Cells were then induced by adding 40% galactose to a final concentration of 2%. At this time, additional alpha factor was added (400 μl of 10 mM, GenScript). Samples were collected at time points 0, 10, 20, 30, 40, 50, 60, 90, 120 and 150 min after galactose induction. At each time point, 35 ml of culture was taken and added immediately to 37% formaldehyde to a final concentration of 1% for 20 min. Thirteen millilitres were taken for subsequent RNA preparation. Two millilitres were taken for protein preparation by pelleting cells and heating at 95 °C for 5 min in 0.06 M Tris-HCl, pH 6.8, 10% glycerol, 2% SDS, 5% 2-mercaptoethanol and 0.0025% bromophenol blue. All samples were frozen immediately in liquid nitrogen.

**Full Methods** and any associated references are available in the online version of the paper at www.nature.com/nature.

**Received 20 February 2011; accepted 23 February 2012.**


1. Mueller, F., Wach, P. & McNally, J. G. Evidence for a common mode of transcription factor interaction with chromatin as revealed by improved quantitative fluorescence recovery after photobleaching. *Biophys. J.* **94,** 3323–3339 (2008).
2. Yao, J., Munson, K. M., Webb, W. W. & Lis, J. T. Dynamics of heat shock factor association with native gene loci in living cells. *Nature* **442,** 1050–1053 (2006).
3. Stavreva, D. A., Muller, W. G., Hager, G. L., Smith, C. L. & McNally, J. G. Rapid glucocorticoid receptor exchange at a promoter is coupled to transcription and regulated by chaperones and proteasomes. *Mol. Cell. Biol.* **24,** 2682–2697 (2004).
4. Karpova, T. S. *et al.* Concurrent fast and slow cycling of a transcriptional activator at an endogenous promoter. *Science* **319,** 466–469 (2008).
5. MacArthur, S. *et al.* Developmental roles of 21 *Drosophila* transcription factors are determined by quantitative differences in binding to an overlapping set of thousands of genomic regions. *Genome Biol.* **10,** R80 (2009).
6. Dion, M. F. *et al.* Dynamics of replication-independent histone turnover in budding yeast. *Science* **315,** 1405–1408 (2007).
7. van Werven, F. J., van Teeffelen, H. A., Holstege, F. C. & Timmers, H. T. Distinct promoter dynamics of the basal transcription factor TBP across the yeast genome. *Nature Struct. Mol. Biol.* **16,** 1043–1048 (2009).
8. Lieb, J. D., Liu, X., Botstein, D. & Brown, P. O. Promoter-specific binding of Rap1 revealed by genome-wide maps of protein-DNA association. *Nature Genet.* **28,** 327–334 (2001).
9. Piña, B., Fernández-Larrea, J., García-Reyero, N. & Idrissi, F. Z. The different (sur)faces of Rap1p. *Mol. Genet. Genomics* **268,** 791–798 (2003).
10. Buck, M. J. & Lieb, J. D. A chromatin-mediated mechanism for specification of conditional transcription factor targets. *Nature Genet.* **38,** 1446–1451 (2006).
11. Holstege, F. C. *et al.* Dissecting the regulatory circuitry of a eukaryotic genome. *Cell* **95,** 717–728 (1998).
12. Layer, J. H., Miller, S. G. & Weil, P. A. Direct transactivator-transcription factor IID (TFIID) contacts drive yeast ribosomal protein gene transcription. *J. Biol. Chem.* **285,** 15489–15499 (2010).
13. Pelechano, V., Chavez, S. & Perez-Ortin, J. E. A complete set of nascent transcription rates for yeast genes. *PLoS ONE* **5,** e15442 (2010).
14. Polach, K. J. & Widom, J. Mechanism of protein access to specific DNA sequences in chromatin: a dynamic equilibrium model for gene regulation. *J. Mol. Biol.* **254,** 130–149 (1995).
15. Segal, E. & Widom, J. From DNA sequence to transcriptional behaviour: a quantitative approach. *Nature Rev. Genet.* **10,** 443–456 (2009).
16. Lam, F. H., Steger, D. J. & O'Shea, E. K. Chromatin decouples promoter threshold from dynamic range. *Nature* **453,** 246–250 (2008).
17. Pokholok, D. K. *et al.* Genome-wide map of nucleosome acetylation and methylation in yeast. *Cell* **122,** 517–527 (2005).
18. Anderson, J. D., Lowary, P. T. & Widom, J. Effects of histone acetylation on the equilibrium accessibility of nucleosomal DNA target sites. *J. Mol. Biol.* **307,** 977–985 (2001).
19. John, S. *et al.* Chromatin accessibility pre-determines glucocorticoid receptor binding patterns. *Nature Genet.* **43,** 264–268 (2011).
20. Zanton, S. J. & Pugh, B. F. Changes in genomewide occupancy of core transcriptional regulators during heat stress. *Proc. Natl Acad. Sci. USA* **101,** 16843–16848 (2004).
21. Kaplan, N. *et al.* The DNA-encoded nucleosome organization of a eukaryotic genome. *Nature* **458,** 362–366 (2009).
22. Koerber, R. T., Rhee, H. S., Jiang, C. & Pugh, B. F. Interaction of transcriptional regulators with specific nucleosomes across the Saccharomyces genome. *Mol. Cell* **35,** 889–902 (2009).
23. Ganapathi, M. *et al.* Extensive role of the general regulatory factors, Abf1 and Rap1, in determining genome-wide chromatin structure in budding yeast. *Nucleic Acids Res.* **39,** 2032–2044 (2011).
24. Mukherjee, S. *et al.* Rapid analysis of the DNA-binding specificities of transcription factors with DNA microarrays. *Nature Genet.* **36,** 1331–1339 (2004).
25. Bosisio, D. *et al.* A hyper-dynamic equilibrium between promoter-bound and nucleoplasmic dimers controls NF-κB-dependent gene activity. *EMBO J.* **25,** 798–810 (2006).
26. Voss, T. C. *et al.* Dynamic exchange at regulatory elements during chromatin remodeling underlies assisted loading mechanism. *Cell* **146,** 544–554 (2011).
27. McNally, J. G., Muller, W. G., Walker, D., Wolford, R. & Hager, G. L. The glucocorticoid receptor: rapid exchange with regulatory sites in living cells. *Science* **287,** 1262–1265 (2000).
28. Perlmann, T., Eriksson, P. & Wrange, O. Quantitative analysis of the glucocorticoid receptor-DNA interaction at the mouse mammary tumor virus glucocorticoid response element. *J. Biol. Chem.* **265,** 17222–17229 (1990).
29. Gorski, S. A., Snyder, S. K., John, S., Grummt, I. & Misteli, T. Modulation of RNA polymerase assembly dynamics in transcriptional regulation. *Mol. Cell* **30,** 486–497 (2008).
30. Rossetti, L. *et al.* Specific interactions of the telomeric protein Rap1p with nucleosomal binding sites. *J. Mol. Biol.* **306,** 903–913 (2001).


**Supplementary Information** is linked to the online version of the paper at www.nature.com/nature.

**Acknowledgements** We thank T. Kaplan and O. Rando for help with their turnover model, T. Palpant and S. Adar for help with time course experiments, and A. Leonardo Iniguez and H. Rosenbaum of Roche Nimblegen for pre-release custom HD4 12-plex microarrays. This work was supported by the US National Institutes of Health (NIH) Grant R01-GM072518 (to J.D.L.), and the intramural program of the NIH, National Cancer Institute, Center for Cancer Research (to J.G.M. and F.M.). F.M. was also supported in part by the Region Ile-de-France in the framework of C'Nano IdF, the nanoscience competence center of Paris Region.

**Author Contributions** C.R.L., S.E.H. and J.D.L. designed the study. C.R.L. and S.E.H. performed the experiments. F.M. developed and implemented the binding dynamics model. C.R.L., F.M., J.G.M. and J.D.L. performed data analysis. C.R.L., F.M., J.G.M. and J.D.L. wrote the paper.

**Author Information** Data has been deposited in the Gene Expression Omnibus under accession numbers GSE32351 (ChIP-on-chip data), GPL14612 (ChIP platform), GSM677030–GSM677033 (RNA expression array data) and GPL4414 (expression platform). Reprints and permissions information is available at www.nature.com/reprints. The authors declare no competing financial interests. Readers are welcome to comment on the online version of this article at www.nature.com/nature. Correspondence and requests for materials should be addressed to J.D.L. (jlieb@bio.unc.edu).

## METHODS

**Strain construction.** The *RAP1* gene and promoter was cloned into the pRS403 plasmid and integrated by homologous recombination into the *HIS3* locus of the BY4741 *S. cerevisiae* strain. The two copies of *RAP1* were then sequentially tagged using the 9× Myc epitope from pYM20:hphNT1 at the *HIS3* copy of *RAP1* and the 3× Flag tag from p3Flag-KanMX at the endogenous *RAP1* copy. The *HIS3* copy of the *RAP1* promoter was replaced using homologous recombination by amplifying the GALL:*natNT2* promoter from the pYM-N27 plasmid. Integrations were confirmed using PCR and western blot analysis. The *BAR1* gene was knocked out by homologous recombination using a *LEU2* gene amplified from pRS405.

**Time course.** Yeast strains were grown overnight in YPD (yeast extract 1%, peptone 2% and dextrose 2%) and used to inoculate 800 ml of YPR (yeast extract 1%, peptone 2% and raffinose 2%) to an attenuance at 600 nm ($D_{600\ nm}$) of 0.2 (Genesys 20 Spectrophotometer) in a 4-l Erlenmeyer flask. These cells were grown to an $D_{600}$ of 0.4 and subsequently arrested using 5 μM alpha factor (400 μl of 10 mM, GenScript) until 95% of the yeast cells were unbudded (~3 h). Cells were then induced by adding 40% galactose to a final concentration of 2%. At this time, additional alpha factor was added (400 μl of 10 mM, GenScript). Samples were collected at time points 0, 10, 20, 30, 40, 50, 60, 90, 120 and 150 min after galactose induction. At each time point, 35 ml of culture was taken and added immediately to 37% formaldehyde to a final concentration of 1% for 20 min. Thirteen millilitres were taken for subsequent RNA preparation. Two millilitres were taken for protein preparation by pelleting cells and heating at 95 °C for 5 min in 0.06 M Tris-HCl, pH 6.8, 10% glycerol, 2% SDS, 5% 2-mercaptoethanol and 0.0025% bromophenol blue. All samples were frozen immediately in liquid nitrogen.

**Turnover model.** A mathematical model is required to interpret the data, and to obtain binding turnover rates. We used a modified version of a histone H3 turnover model[6]. The original H3 turnover model assumed that there was no competitor protein present before its induction[6]. We were also unable to detect the presence of the Rap1 competitor protein before induction using western blot analysis. Nevertheless, at each locus we consistently measured a non-zero competitor signal from the microarray even before the competitor was induced. This probably reflects the nonspecific background of our microarrays. Most of the steps that could contribute to this noise—for example, non-specific pull down from the beads, site-specific variations in the DNA amplification or nonspecific binding bias in hybridization—would affect the constitutive and competitor signal equally, and therefore we assume for simplicity that the total nonspecific background signal is approximately the same for the constitutive signal and for the competitor signal in our modified turnover model. We assume that at each binding site the measured immunoprecipitation signal (mIP(t)) is the true immunoprecipitation signal (IP(t)) plus the background (BGD(t)):

$$\mathrm{mIP(t)} = \mathrm{IP(t)} + \mathrm{BGD(t)} \tag{1}$$

We assume that at the beginning of the experiment (before induction) the true IP signal of the competitor is zero. The background signal at the start of the experiment is therefore the signal measured for the competitor protein A at time 0:

$$\mathrm{mIP_A(0)} = \mathrm{BGD(0)} \tag{2}$$

The measured background signal will generally be time-dependent because our data showed that the measured raw intensities of the immunoprecipitation signals for the constitutive and competitor Rap1 proteins fluctuated from one time point to the next, even though their relative proportions remained roughly the same. This suggests that there are systematic variations in either the ChIP conditions or the microarray imaging conditions from one time point to the next, which would also probably influence the background signal.

The systematic changes in either the ChIP or imaging conditions can be quantified by comparing the total signal of constitutive Rap1 plus competitor Rap1 at each binding site as a function of time. We assume that the addition of competitor does not change total occupancy[6] (Supplementary Figs 3 and 4). Thus, at each binding site, the ratio of the total signal (constitutive plus competitor Rap1) at time *t* versus time 0 generates a scaling factor to account for systematic fluctuations over time. This scaling factor (the part in brackets in equation (3)) can be used to calculate the background signal at time t based on the background at time 0:

$$\mathrm{BGD(t)} = \mathrm{BGD(0)} \times \left( \frac{\mathrm{IP_A(t)} + \mathrm{IP_B(t)}}{\mathrm{IP_A(0)} + \mathrm{IP_B(0)}} \right) \tag{3}$$

With this formula, we can calculate an occupancy ratio in the presence of background signal. First note that the occupancy ratio $R(t)$ in the absence of background is defined as the ratio of the immunoprecipitates of the competitor and constitutive signals:

$$\mathrm{R(t)} = \mathrm{IP_A(t)}/\mathrm{IP_B(t)} \tag{4}$$

We define a measured occupancy ratio mR(t) that includes the background signal:

$$\mathrm{mR(t)} = \mathrm{mIP_A(t)}/\mathrm{mIP_B(t)} = [\mathrm{IP_A(t)} + \mathrm{BGD(t)}]/[\mathrm{IP_B(t)} + \mathrm{BGD(t)}] \tag{5}$$

where the second equality arises by substitution from equation (1), assuming that the background is the same in the competitor and constitutive signals. Using equations (2), (3) and (4), equation (5) can be rewritten as:

$$\mathrm{mR(t)} = [\mathrm{R(t)} + \mathrm{C_0}(1 + \mathrm{R(t)})]/[1 + \mathrm{C_0}(1 + \mathrm{R(t)})] \tag{6}$$

where $C_0 = \mathrm{mIP_A(0)}/(\mathrm{IP_A(0)} + \mathrm{IP_B(0)})$. This constant can be expressed in terms of measurable quantities by using equations (1), (2) and the previously stated assumption $\mathrm{IP_A(0)} = 0$ to yield:

$$C_0 = \frac{\mathrm{mR(0)}}{1 - \mathrm{mR(0)}} \tag{7}$$

where mR(0) is the measured occupancy ratio at time 0. In practice, we calculated $C_0$ by averaging over the first three time points, and found that they all showed no detectable competitor signal. With this estimate of $C_0$, equation (6) enables an occupancy ratio to be calculated in the presence of a microarray background signal by using the occupancy ratio $R_t$ calculated in the absence of background[6].

R(t) is the probability that a locus is occupied by the competitor protein divided by the probability that it is occupied by the constitutive protein[6]. If $P$ is the probability that the competitor occupies a given locus, then the probability that the constitutive protein occupies the locus is $1 - P(t)$, and so R(t) becomes:

$$R(t) = \frac{P(t)}{1 - P(t)} \tag{8}$$

This probability satisfies the following differential equation[6]:

$$\frac{\mathrm{d}}{\mathrm{d}t} P(t) = \lambda \left( \frac{A(t)}{A(t) + B(t)} - P(t) \right) \tag{9}$$

Here $\lambda$ is the turnover rate at each locus, and $A(t)$ and $B(t)$ are the cellular concentrations of the free competitor and constitutive proteins. We measured $A(t)$ and $B(t)$ at all time points using western blot analysis. To determine the turnover rate $\lambda$ for each locus we tuned $\lambda$ to fit the measured occupancy ratio mR(t) at that locus. Specifically, we varied $\lambda$ in equation (9) such that the value of $R(t)$ obtained from equation (8) yields the best fit to our measured occupancy ratio when $R(t)$ is substituted into equation (6).

The modified turnover model (equation (6)) was implemented in Matlab 2009b (The MathWorks) and equation (9) was solved numerically using the *ODE45* function. The Matlab routine 'lsqcurvefit' was used to fit the models to experimental data and extract the turnover rate $\lambda$. We sampled a range of different starting guesses to avoid the detection of local minima. The Matlab source code for the modified turnover model is available online (http://code.google.com/p/ccc-process/).

**Plasmids.** The following plasmids were used in generation of the Rap1 turnover strain: pRS403 (ref. 31), pRS405 (ref. 31), pYM20:hphNT1 (ref. 32), p3FLAG-KanMX (ref. 33) and pYM-N27 (ref. 32).

**Chromatin immunoprecipitation and DNA amplification.** Chromatin immunoprecipitation was performed on whole-cell extract from crosslinked cells as described previously, using anti-Flag (M2, Sigma), anti-Myc (clone 9E10, Millipore), and anti-Rap1 (y-300, Santa Cruz Biotechnology)[8]. Immunoprecipitated and/or input DNA was amplified using the GenomePlex Complete Whole-Genome Amplification (WGA) kit (WGA2-50RXN, Sigma) and then re-amplified using GenomePlex WGA Reamplification Kit (WGA3-50RXN, Sigma) using the manufacturer's protocols. DNA was purified using Zymo columns according to the manufacturer's instructions (Zymo Research).

**Hybridization and processing of data from high-resolution HD4 microarrays.** For Nimblegen high-resolution HD4 microarrays, amplified ChIP material was sent directly to Nimblegen where it was labelled and hybridized according to protocols in chapters 3 and 4 of the NimbleGen Arrays User's Guide ChIP-chip Analysis, Version 3.1, 27 May 2008. Bi-weight mean scaled ratios are used as input for lowess normalization. All HD4 array data are deposited in the Gene Expression Omnibus (GEO) under accession GSE32351.

**Modified lowess normalization.** Standard lowess normalization results in depressed binding ratios at the most highly enriched probes in ChIP-chip experiments. We therefore implemented a modified lowess normalization designed specifically for ChIP-chip based on the method described previously[7]. Our method varied from the previously published method[7] in that we defined the 'enriched' group of probes based on the sites that we used to define Rap1 target enrichment for our turnover time course. We excluded all probes within ±2,000 bp of a Rap1 binding site, and used all remaining probes as the reference group to calculate the lowess function for normalization (Supplementary Fig. 8a–d). Each time point is normalized separately but we use the same group of reference probes for the normalization. Although we believe that using this modified lowess normalization

approach is the most appropriate way to normalize the data, we find qualitative and quantitatively similar Rap1 turnover values without normalization (data not shown).

**Hybridization and processing of data from low-resolution PCR-based arrays.** One microgram of amplified DNA was labelled with either 2′-deoxyuridine, 5′-triphosphate (dUTP) Cy5 (PA55022, GE Healthcare) or Cy3 (PA53022, GE Healthcare) for low-resolution PCR-based arrays. Purified labelled DNA was hybridized to PCR-based arrays representing the whole yeast genome and covering all coding and non-coding regions at an average resolution of approximately 800 bp (ref. 10). The time course was performed in duplicate, one in each dye orientation, with the Myc and Flag samples then comparatively hybridized to an array for each time point. Arrays were scanned using an Axon 4000B scanner and analysed using Genepix 6.0 software (Axon). Only spots with <10% saturated input pixels and a signal intensity of greater than 500 (background-corrected sum of medians for both channels) were used for the analysis. Data were further normalized in the UNC microarray database with the normalized median $\log_2$ ratio of Rap1–Myc/Rap1–Flag being used for further analysis. All low-resolution array data are deposited in GEO under accession GSE27377. We did not use these ChIP-chip data in any of our analyses except in Supplementary Fig. 3.

**Reverse transcription, complementary-DNA labelling and expression arrays.** Total RNA was extracted by the hot phenol method as previously described[34]. Total RNA (30 μg) was reverse transcribed into cDNA using reagents and protocols provided with SuperScript II reverse transcriptase (Invitrogen; Cat. No. 18064-014) containing an amino-allyl-dDUTP mix (50× aa-dUTP mixture; 1 mg amino-allyl dUTP (Sigma)) dissolved with 32 μl of 100-mM dATP, dGTP, dCTP, 12.7 μl of 100-mM dTTP, and 19.3 μl of $dH_2O$, and an anchored oligo dT primer (22-mer; IDT). Reactions were incubated for 2 h at 42 °C, then heated at 95 °C for 5 min and snap cooled on ice. RNA was hydrolysed by addition of 13 μl of 1-N NaOH and 1 μl of 0.5-M EDTA followed by incubation at 67 °C. Reactions were then neutralized with 50 μl of 1 M HEPES pH 7.5. cDNA was purified on Zymo columns (Zymo Research; D4003) using a seven-volume excess of DNA binding buffer. cDNA was eluted from columns using 5 μl of 50-mM sodium bicarbonate pH 9.0. cDNA was fluorescently labelled using Amersham CyDye Post-Labelling Reactive Dye Packs (RPN5661). Each dye pack was resuspended in 11 μl DMSO and 3 μl of mixture was used per reaction. Cy dyes and aa-dUTP cDNAs were allowed to couple for 2 h in the dark. Labelled cDNAs were cleaned up using Zymo columns with a seven-volume excess of DNA binding buffer and eluted with 10 mM Tris-Cl pH 8.0 and hybridized to arrays as described previously.

For comparative hybridization, input genomic DNA from the experimental Rap1 turnover strain was extracted using phenol chloroform. Four micrograms of genomic DNA was denatured at 100 °C with 10 μg of random hexamer (IDT) then snap cooled on ice for 10 min. Samples were then incubated with 50 units of Klenow (exo-) (New England Biolabs (NEB)) and 1× Buffer 2 (NEB) in a total volume of 50 μl at 37 °C for 2 h. Samples were cleaned up with Zymo columns, eluted in 5 μl of 5-mM sodium bicarbonate pH 9.0 and coupled to Cy dyes as for cDNA. Expression studies were performed on PCR-based arrays that were prepared, processed and analysed as for the low-resolution ChIP arrays[10].

**Defining regions of Rap1 enrichment.** Rap1 ChIP–seq data from yeast strain BY4741 grown in YPD (yeast extract 1%, peptone 2% and dextrose 2%) were used to determine precise sites of Rap1 binding. Peaks and peak summits were identified using model-based analysis for ChIP-Seq (MACS) with a bandwidth of 300 and a *P*-value cutoff of $1 \times 10^{-5}$. Peaks in our turnover data set were identified on total Rap1 occupancy at time 0 using Peakpicker[35] to ensure that we identified all Rap1 peaks that were present in our turnover conditions. For analysis, we then used only MACS Chip-seq peak regions that had at least 1 bp of overlap with our time-course peaks, and a *z* score of >1.5 at time 0. Seven regions with a *z* score of >1.5 at time 0 that were identified at time 0 of the Rap1 time course but not of the ChIP–seq experiment were also included to ensure full representation of Rap1-enriched regions in our experiment. Of the 457 total Rap1 peak regions identified, 18 were not analysed. Fifteen targets had an estimated residence time of under 500 s, which is too short to measure with our system (Supplementary Fig. 6). Three targets that had residence times that exceeded $1 \times 10^4$ s and showed exceptionally poor fits to the model were also excluded. The average $\log_2$ Myc/Flag level for all probes which fell within ±150 bp of peak summits were averaged to generate a Myc/Flag value for each time point for each target. On average, eight probes contributed to the Myc/Flag signal for Rap1 targets. Peak summits were used to assign target regions to promoters or coding regions for further analysis.

Telomeric regions were tiled using only uniquely mapping probes, making signal discontinuous in these regions and making peak calling difficult. For this reason, telomeres were defined by annotations from the *Saccharomyces* genome database (http://www.yeastgenome.org/). We excluded telomeres from any analysis that relied on our turnover metric because they contain many arrayed Rap1 binding sites within their AC-rich repeats. In theory, as the number of Rap1-binding sites detected by an individual microarray probe increases, the probability that either isoform of Rap1 will be detected at that probe increases. This violates some assumptions of our turnover metric, which would theoretically lead to artificially short residence-time estimates. Despite this, empirically we see no relation between Rap1 residence times and motif number or density (Supplementary Fig. 10).

**Motif discovery.** The 439 Rap1-bound target regions (excluding telomeres) were placed into four categories based on their turnover properties: longest (110 targets), long (110 targets), short (110 targets) and shortest (109 targets). The DNA sequences for each Rap1 target region in each group were then used as input for the web-based interface for BioProspector[36] (http://ai.stanford.edu/~xsliu/BioProspector/). Default parameters were with the exception of the width of the first motif block, which was changed to '13' and '*S. cerevisiae* intergenic' was used as a genome-background model. Rap1's telomeric motif was determined from the full telomeric sequences of the 26 telomeres that were uniquely mappable on our arrays. Weblogo[37] (http://weblogo.berkeley.edu/logo.cgi) was used to generate a visual representation of the position–weight matrix output from Bioprospector. The 439 Rap1 targets were similarly grouped by their occupancy properties to determine Rap1 motifs for Rap1 targets grouped by occupancy. The default settings on the motif scanning program Clover[38] were used to detect Rap1 motifs genome-wide using a previously published Rap1 position–weight matrix[10].

**External data sets.** Values from existing data sets with a one-to-one correspondence to the arrayed elements in our study were used as published. For data sets derived from arrays that did not match our probe set, $\log_2$ ratios and *z* scores were calculated for each array probe, for each replicate of the external data set. *Z* scores were defined as the number of standard deviations that a probe's $\log_2$ ratio was from the mean $\log_2$ ratio of all probes on the array. In cases with several replicates, average *z* scores were used to represent each probe. To map the data back to our experiments, the average *z* scores of the array probes for the specific data set that were contained within the promoter or coding region assigned to each Rap1 target were used for comparison. For histone H3 turnover data, the highest value for a probe that fell within promoters associated with peak summits for target regions was used for our analysis[6]. For Rap1 nucleosome interaction data we summed all the detected interactions that fell within each Rap1 target region.


31. Sikorski, R. S. & Hieter, P. A system of shuttle vectors and yeast host strains designed for efficient manipulation of DNA in *Saccharomyces cerevisiae*. *Genetics* **122,** 19–27 (1989).
32. Janke, C. *et al.* A versatile toolbox for PCR-based tagging of yeast genes: new fluorescent proteins, more markers and promoter substitution cassettes. *Yeast* **21,** 947–962 (2004).
33. Gelbart, M. E., Rechsteiner, T., Richmond, T. J. & Tsukiyama, T. Interactions of Isw2 chromatin remodeling complex with nucleosomal arrays: analyses using recombinant yeast histones and immobilized templates. *Mol. Cell. Biol.* **21,** 2098–2106 (2001).
34. Hoffman, C. S. in *Current Protocols in Molecular Biology*, Vol. 2 (eds Ausubel, F.M. *et al.*) 13.11.1–13.11.4 (John Wiley and Sons, 1997).
35. Cesaroni, M., Cittaro, D., Brofzi, A., Pelicci, P. G. & Luzi, L. CARPET: a web-based package for the analysis of ChIP-chip and expression tiling data. *Bioinformatics* **24,** 2918–2920 (2008).
36. Liu, X., Brutlag, D. L. & Liu, J. S. BioProspector: discovering conserved DNA motifs in upstream regulatory regions of co-expressed genes. *Pac. Symp. Biocomput.* **6,** 127–138 (2001).
37. Crooks, G. E., Hon, G., Chandonia, J. M. & Brenner, S. E. WebLogo: a sequence logo generator. *Genome Res.* **14,** 1188–1190 (2004).
38. Frith, M. C. *et al.* Detection of functional DNA motifs via statistical over-representation. *Nucleic Acids Res.* **32,** 1372–1381 (2004).